doi:10.1016/S0022-2836(02)01272-X J. Mol. Biol. (2003) 325, 433–442

JMB

Available online at www.sciencedirect.com

SCIENCE DIRECT®

Solution Structure of a DNA Duplex Containing 8-Hydroxy-2′-Deoxyguanosine Opposite Deoxyguanosine

Varatharasa Thiviyanathan[1], Anoma Somasunderam[1], Tapas K. Hazra[2] Sankar Mitra[2] and David G. Gorenstein[1,2]*

[1]*Sealy Center for Structural Biology, Department of Human Biological Chemistry and Genetics, University of Texas Medical Branch 301 University Blvd. Galveston, TX 77555-1157 USA*

[2]*Sealy Center for Molecular Sciences, Department of Human Biological Chemistry and Genetics, University of Texas Medical Branch Galveston, TX 77555-1079 USA*

**Corresponding author*

Deoxyguanosine residues are hydroxylated by reactive oxygen species at the C-8 position to form 8-hydroxy-2′-deoxyguanosine (8-OG), one of the most important mutagenic lesions in DNA. Though the spontaneous G:C to C:G transversions are rare events, the pathways leading to this mutation are not established. An 8-OG:G mispair, if not corrected by DNA repair enzymes, could lead to G:C to C:G transversions. NMR spectroscopy and restrained molecular dynamics calculations are used to refine the solution structure of the base mismatch formed by the 8-OG:G pair on a self complementary DNA dodecamer duplex d(CGCGAATT$^{8\text{-O}}$-GGCG)$_2$. The results reveal that the 8-OG base is inserted into the helix and forms Hoogsteen base-pairing with the G on the opposite strand. The 8-OG:G base-pairs are seen to be stabilized by two hydrogen bonding interactions, one between the H7 of the 8-OG and the O6 of the G, and a three-center hydrogen bonding between the O8 of the 8-OG and the imino and amino protons of the G. The 8-OG:G base-pairs are very well stacked between the Watson–Crick base-paired flanking bases. Both strands of the DNA duplex adopt right-handed conformations. All of the unmodified bases, including the G at the lesion site, adopt *anti* glycosidic torsion angles and form Watson–Crick base-pairs. At the lesion site, the 8-OG residues adopt *syn* conformations. The structural studies demonstrate that 8-OG(*syn*):G(*anti*) forms a stable pair in the interior of the duplex, providing a basis for the *in vivo* incorporation of G opposite 8-OG. Calculated helical parameters and backbone torsional angles, and the observed ^{31}P chemical shifts, indicate that the structure of the duplex is perturbed near lesion sites, with the local unwinding of the double helix. The melting temperature of the 8-OG:G containing duplex is only 2.6 deg. C less than the t_m of the unmodified duplex.

© 2003 Elsevier Science Ltd. All rights reserved

Keywords: oxidative DNA damage; 8-oxo guanine; MutY; DNA repair; transversions

Introduction

Oxidative DNA damage is thought to play a significant role in cancer and aging. Deoxyguanosine residues in DNA are hydroxylated by reactive oxygen species at the C-8 position to form 8-hydroxy-2′-deoxyguanosine (8-OG), the most common product of oxidative damage to DNA. 8-OG is formed also by reaction of singlet oxygen or hydroxyl radicals with dGTP in the cellular dNTP pool, and can be incorporated into DNA by DNA polymerases. In its monomeric form, 8-OG adopts several tautomeric forms. However, the 6,8-dioxo species is shown to be the predominating form under physiological conditions.[1,2] 8-OG has received considerable attention for its demonstrated mutagenic and carcinogenic potential. Fourier transform-infrared

Abbreviations used: 8OG, 8-hydroxy-2′-deoxyguanosine; NOE, nuclear Overhauser effect; NOESY, NOE spectroscopy; r-MD, restrained molecular dynamics; MORASS, multiple Overhauser relaxation analysis and simulation; Gh, guanidinohydantoin; Sp, spiroiminohydantoin; TOCSY, total correlated spectroscopy; DMT, 5′-dimethoxytrityl.

E-mail address of the corresponding author: david@nmr.utmb.edu

0022-2836/03/$ - see front matter © 2003 Elsevier Science Ltd. All rights reserved

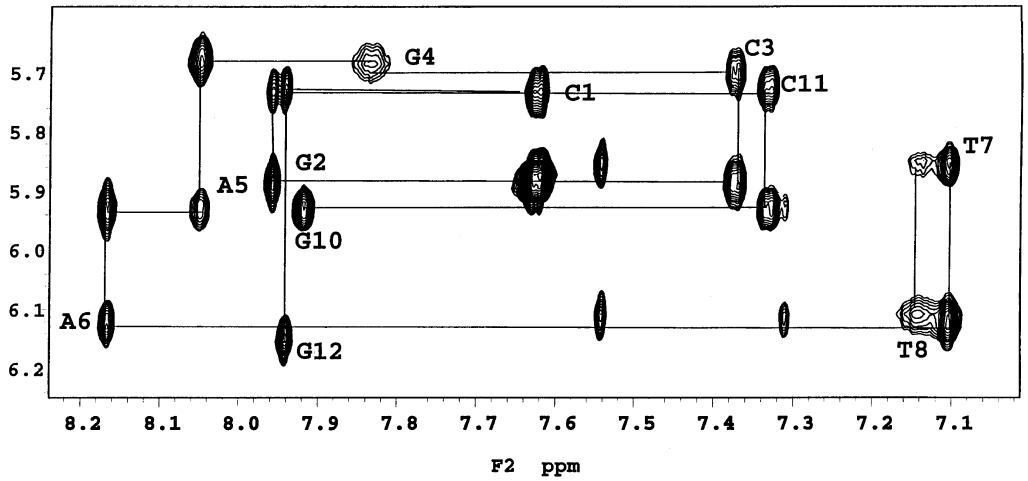

Figure 1. Aromatic to anomeric proton region of the 2D NOESY spectra obtained with the 250 ms mixing time at 10 °C.

spectroscopic studies showed that single 8-oxo-purine lesions cause marked changes in base interactions and backbone conformations in a 25 base single stranded DNA.[3] These studies showed that a single 8-oxo purine lesion in DNA strands can cause significant structural perturbations at the replication fork, and thus affect the proof-reading capacity of DNA polymerases. The 8-oxo lesions in DNA could significantly alter the DNA strand conformation and thus affect the replication and the transcription processes. Earlier reports indicate that 8-OG causes mis-replication at the lesion site, and at neighboring bases.[4] In *in vitro* experiments, the 8-OG is shown to form base-pairs with all four dNTPs with an almost equal frequency.[4] However, a later study showed that the 8-OG pairs preferentially with A and C.[5] Although spontaneous G:C → C:G transversions are rare events, the frequency of G:C → C:G transversions increases significantly upon exposure to ionizing radiation and oxidizing chemicals.[6,7] The biological pathways leading to this transversion remain uncertain. When the 8-OG pairs with G, and the mismatch is not corrected during DNA replication, it could lead to G:C → C:G transversions. 8-OG:G can arise by the oxidation of G:G base mismatches that occur during DNA replication. We earlier reported the discovery of the 36 kDa OGG-2, which prefers to act on 8-OG paired with G and A.[8] The *Escherichia coli* DNA repair enzyme MutY has a guanine-DNA glycosylase activity that acts on 8-OG:G mispairs.[9] The presence of DNA repair enzymes that can act on 8-OG:G mismatches shows that this base mis-pairing could occur *in vivo*. Some other forms of oxidized G can form a mismatch with G. Recently, it has been reported that one electron oxidation of 8-OG produces guanidinohydantoin (Gh) and spiroiminohydantoin (Sp).[10,11] Both these have been found to pair with G and A, suggesting that Gh and Sp could induce G-T and G-C transversion mutations.

When incorporated into the oligonucleotides, the 8-OG appears to retain the 6,8-diketo tautomeric form.[1] However, the glycosidic angle of the 8-OG residue depends on the nature of the base-pairing partner. Both NMR[12] and crystallographic studies[13] have shown that 8-OG, when base-paired with A, adopts a *syn* conformation and the base-paired A adopts a normal *anti* conformation. In contrast, when paired with C, 8-OG forms normal Watson–Crick base-pairing and both the 8-OG and the base-paired C adopt *anti* conformations, in both crystal[14] and NMR solution structures.[15] The crystal structure reported for a DNA duplex containing 8-OG:C mismatch is very similar to that of the unmodified DNA duplex.[14] Gannett & Sura[16] suggest, on the basis of NMR studies on base-pairs formed between 8-OG and other DNA bases, that the 8-OG adopts a *syn* conformation when it paired with A, T, and G, and retains the *anti* conformation when paired with C.

In an attempt to probe the structure of the base mismatch formed by the 8-OG:G pair, we have used NMR studies coupled with restrained molecular dynamics refinement techniques. The sequence used in the present study, d(CGCG-AATT$^{8\text{-O}}$GGCG)$_2$, is related to the *Eco*RI sequence that has been studied extensively by NMR and crystallography.[17–19]

Results

Assignment of non-exchangeable protons

Sequential assignments were made on the basis of the aromatic-H1′ connectivities and were confirmed by the aromatic–aromatic cross-peaks and aromatic-H2′/H2″/H3′ connectivities. Other sugar protons (H3′, H4′, H5′ and H5″) were assigned independently from the 2D total correlated spectroscopy (TOCSY) and the 50 ms mixing time 2D nuclear Overhauser effect spectroscopy (NOESY) spectra. The adenine H2 protons also gave cross-peaks to the base-paired H1′ protons of the thymidine. The H2 of A5 showed cross-peaks

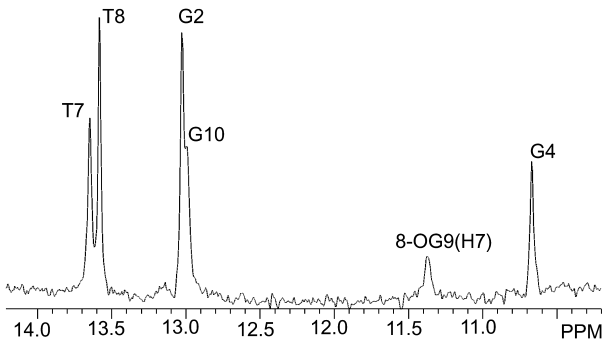

Figure 2. Imino proton region of the 1D proton NMR spectra collected at 10 °C at 750 MHz, showing six resonances. The H1 imino proton of the 8-OG residue was not observed, probably due to exchange with solvent.

to the H1′ of A5 and A6, and a cross-strand cross-peak to the H1′ of the 8-OG residue. The H2 of A6 showed a cross-strand NOE to T19 (H1′). This observed pattern of NOESY peaks is consistent with the duplex adopting the typical right-handed *B*-DNA conformation.[20]

The aromatic/H1′ region of the 2D NOESY spectra taken at 10 °C, is shown in Figure 1. The expected sequential aromatic-H1′ NOESY connectivities were disrupted between T8 and 8-OG9, since the 8-OG residue lacks an aromatic proton. The NOESY cross-peak between the C3–H1′ and G4–H8 is weaker compared to other similar cross-peaks in the duplex. In NOESY data collected at 25 °C, this cross-peak is not observed. (The chemical shifts are available in Table S1 of the Supplementary Material and are deposited at the Wisconsin data bank† with the accession number 5385.) All the observed intra-residue H8/H6 to H1′ NOESY cross-peaks were less intense than the intra H6–H5 cross-peaks, and the intra-residue H8/H6 to H2′ cross-peaks were stronger than the cross-peaks to other sugar protons, indicating that all the unmodified residues, including the G opposite to the 8-OG residue, adopt *anti* conformation in the DNA duplex.

Exchangeable proton assignments

The exchangeable amino and imino protons were assigned from the 1D and 2D spectra collected in H_2O. In the imino proton region, six resonances were observed between 10.70 ppm and 13.65 ppm (Figure 2). The T7 and T8 imino protons were assigned on the basis of the strong T-imino to A H2 cross-peaks. The resonances at 13.05 ppm and 13.01 ppm were assigned, from the strong cross-peaks between the G-imino and C-amino protons, to the imino protons of G2 and G10, respectively. The peak at 10.70 ppm is assigned to the G4 H1 proton, on the basis of the observed strong cross-peak to the G4 amino proton at 5.60 ppm. The G4 amino protons were assigned independently from the cross-peaks between these amino protons and the H1′ and the H5′ protons of the A5 residue. The H1 imino proton of the G4 at 10.70 ppm showed a strong cross-peak to the resonance at 11.38 ppm, which is assigned to the H7 imino proton of the 8-OG residue. The resonance at 11.38 ppm is broad, and did not show any cross-peak to amino protons. In the *syn* conformation, the 8-OG residue's H1 imino and the amino protons are exposed to solvent, and not hydrogen bonded and would not be detected in the spectra. The G4–H1 and 8-OG H7 showed cross-peaks to the H2 of A5, and the observed intensities of these peaks is consistent with the distances observed in the final averaged structure.

NOESY cross-peaks involving 8-OG residues

As seen in Figure 1, a sequential H1′–H8 cross-peak was not observed between T8 and 8-OG9, since there is no H8 proton in the 8-OG residue. However, the H1′, H2′, H2″, and H3′ sugar protons of the 8-OG9 residue showed cross-peaks to the H8 of the G10 residue, indicating that the 8-OG residues are very well stacked in the helix. The H1′ of the 8-OG showed a strong cross-peak to the H5′ proton of the G10, and the H5′ of 8-OG showed a NOESY cross-peak to the H1′ of T8. The H2′ proton of the 8-OG9 resonance shows an unusually downfield shift, resonating at 3.26 ppm. Downfield-shifted H2′ signals are observed for the G residues when they are in the *syn* conformation, where the lone pair electrons on N3 come close to the C2′–H2′ bond.[21,22] However, the downfield shift is not considered as evidence for the *syn* conformation. The A5 H2 showed cross-strand NOE cross-peaks to the H1′, and H3′ sugar protons of the 8-OG residues.

Assignment of ^{31}P signals

Phosphorus chemical shifts, influenced strongly by the backbone torsional angles, provide valuable information on the phosphate ester backbone conformation and a measure of relative populations of B_I and B_{II} conformations.[23,24] Phosphorus signals were assigned *via* a 2D heteronuclear correlation NMR spectra (Figure 3).[25] Since the H3′ and H4′ resonances had been assigned *via* the TOCSY and NOESY experiments, it was possible to assign ^{31}P peaks through their connectivities *via* scalar coupling to the H3′ and H4′ protons. Downfield-shifted ^{31}P resonance, observed for the OG9 phosphorus atom (numbering corresponds to the phosphate position at the 3′ side of the residue), indicates significant population of the B_{II} conformation for this phosphorus atom.[26] This is reflected in the backbone torsional angles calculated for the final averaged structure. The major structural variation responsible for the ^{31}P shift perturbations appears to be the P–O ester conformation, defined by the backbone torsional angles ζ and α, which

† http://bmrb.wisc.edu

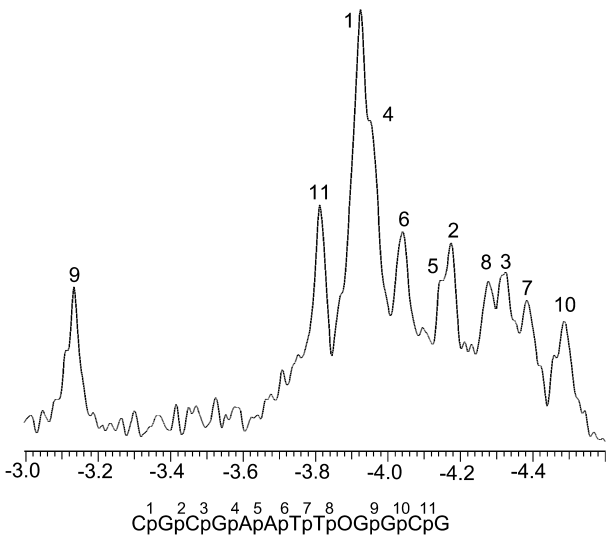

Figure 3. The 1D ^{31}P NMR spectra (proton decoupled) and phosphate assignments of the 8-OG:G containing 12-mer duplex. Data collected at 240 MHz at 25 °C. Numbering, shown below the Figure, corresponds to phosphate position at the 5′ end of the residue. The phosphorus resonances were referenced to TMP at 0.0 ppm.

respond to changes in the local helical structure (e.g. helical twist and roll angle).[24,26,27]

Structure refinement

Progress of the iterative refinement was monitored by several indicators and the final statistics are listed in Table 1. The %rms (volume) and the $Q^{(1/6)}$ factor are useful measures of quality of fit, as they are sensitive to weaker cross-peaks that correspond to longer-range (e.g. inter-residue) distances. The *R*-factor is regarded as a poorer measure of the quality of the refined structure, since it is often dominated by the largest cross-peaks. The %rms (volume), *R*-factor and $Q^{(1/6)}$ factor, started at relatively higher values and gradually settled down to lower values, as the refinement progressed. Both the total energy and the constraint energy increased in values, as the error bars and force constants on the restraints were tightened during the refinement. A stereo-view of the final averaged structure is shown in Figure 4.

Table 1. Structure refinement statistics (final averaged structure)

A. *NMR derived distance constraints*	
Inter-residue[a]	143
Intra-residue[a]	132
Cross-strand	8
H-bond restraints	12
B. *Structure statistics*	
MORASS figures of merit[b]	
%rms (volumes)	74.6
R-factor	0.4468
$Q^{(1/6)}$ factor	0.0726
Distance violations	
> 1.0 Å	0
> 0.5 Å < 1.0 Å	4
> 0.3 Å < 0.5 Å	5
rms deviations from ideal covalent geometry	
Bond length (Å)	0.0061
Bond angle (deg.)	4.01

[a] Restraints per strand.
[b] For definitions, see Materials and Methods.

Helical parameters and the backbone torsional angles for the final averaged structure were calculated using the CURVES program.[28] All the sugar puckers show either $C_{2'}$-*endo* or $C_{1'}$-*exo*, indicating the duplex adopting a general *B*-like DNA conformation. Analysis of the inter-base-pair helical parameters shows structural perturbations at and near the lesions. The helical rise is significantly higher (~5 Å compared to ~3.5 Å for other base-pairs) on the 5′ side of the 8-OG and significantly lower (~1.8 Å) at the 3′ side of the 8-OG residue. The helical twist shows significant deviations at the lesion site. The 8-OG:G mismatched pairs are shifted significantly from the neighboring base-pair, shift value of 4.4(± 0.4) Å, compared to shift values of less than 1 Å for the rest of the base-pairs in the duplex. The helical twist values are significantly lower at the lesion site (20° compared to the averaged value of 32°), indicating local unwinding of the helix at the lesion site. It should be noted that no torsional angle restraints were used during the refinement to allow propeller twist. The torsional angles α, β, and γ are largely constrained to values *gauche*$^-$ (−60°), *trans* (180°) and *gauche* (+60°), whereas significant variations are observed for ζ, ε, and δ. The greatest variation is observed for ζ. The backbone gets narrower near the lesion site, as evidenced by the shorter inter-strand phosphorus–phosphorus distance of 16.7 Å compared to the 18.2(±0.7) Å for other base-pairs. This may be due to the *syn* conformation of the 8-OG residue. (The backbone torsional angles calculated for the final averaged structure are shown in Table S-II of the Supplementary Material.)

Unwinding of the double helix at the lesion sites is evident by the downfield ^{31}P chemical shift, and the values obtained for the backbone torsional angles and the helical parameters for bases near the 8-OG lesion sites. Unwinding of the helix requires torsion about ε, δ, and ζ to open up the deoxyribose phosphate backbone to span the larger separation between stacked base-pairs. The unwinding of the DNA duplex causes a downfield shift of the ^{31}P signal,[29] as shown in the ^{31}P spectra in Figure 3.

Melting temperatures determined by UV absorbance

Melting temperatures, determined by optically monitored thermal denaturation, are listed in

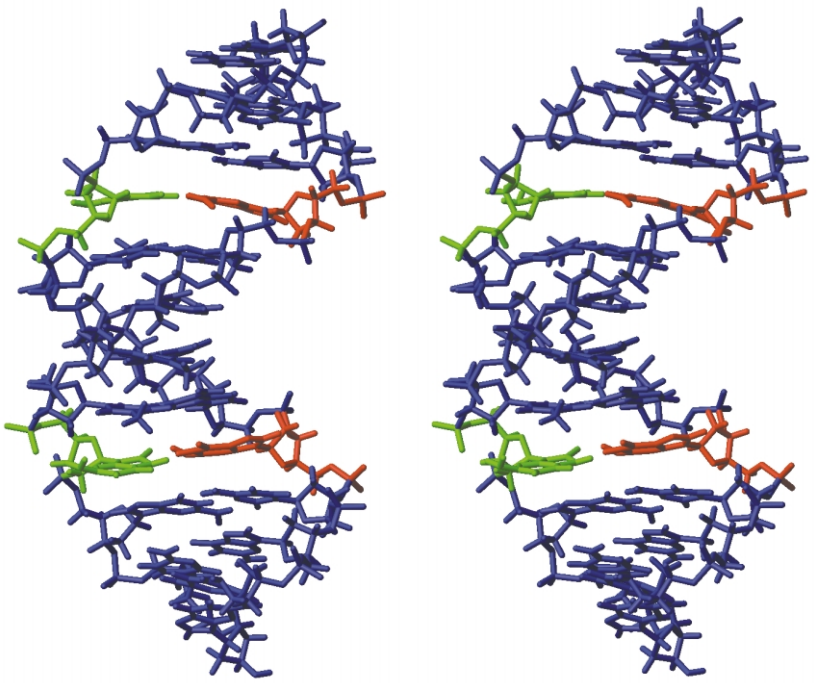

Figure 4. Stereo view of the final averaged structure of the 8-OG:G mismatched 12-mer duplex. The 8-OG residues are shown in green and the base-paired G residues are shown in red.

Table 2. Melting temperatures obtained under identical conditions for the native *Eco* RI 12-mer sequence and the G:G mismatch-containing duplex with the same sequence, were reported previously[30] and are listed in Table 2 for comparison. The melting temperatures indicate that the G:G mismatches are highly destabilizing, and the Δt_m between the G:G and the 8OG:G is 29.2 deg. C. Therefore, the oxidation of a G residue in a G:G mismatch in DNA duplex results in a more stable 8-OG:G mismatch. The t_m for the 8-OG:G mismatch is also higher than the t_m for the 8-OG:A mismatch, indicating that the 8-OG:G mismatch is more stable than the 8-OG:A mismatch.

Discussion

Several NMR and crystal studies are reported on G:G mismatches in DNA duplexes. Earlier predictions of G:G mispair formation with one G in keto and *syn* conformation and the other in enol and *anti* conformation[31] has been ruled out by later structural studies that showed both residues adopting the keto form.[30,32] Several possible pairing schemes were reported for the G:G mismatches.[24,32,33] In general, the G:G mispairs were found to be highly destabilizing, and exhibit considerable conformational heterogeneity at the mismatch site.[30] Molecular modeling studies on a 12-mer duplex having the same sequence as in this study showed the G(*anti*):G(*anti*) conformation to have the lowest energy. However, the energy difference between this conformation and the G(*syn*):G(*anti*) conformation appears to be negligible, suggesting that the G:G mismatches are conformationally less stable and can adopt multiple conformations. NMR studies on G:G mismatches have shown that the mis-paired bases are hydrogen bonded only weakly with different hydrogen bonding patterns, and partially stacked in the helix. The NMR spectra of this 8-OG:G mismatch-containing duplex does not show significant populations of multiple conformations, and the structure appears to be more stable than the reported structures of G:G mismatches.[24,32,33] Melting temperatures obtained from the UV-monitored thermal denaturation experiments (Table 2) shows that the 8-OG:G base-pairs are more stable than the G:G mismatches. The oxidation of G provides a hydrogen bond acceptor at the O8 position that is not available in the case of G. The additional stability of the 8-OG:G mismatch compared to the G:G mismatch, may arise from the *syn* conformation, which orients the O8 of the 8-OG towards the mis-paired G base, to form an additional hydrogen bond.

The melting temperatures and the association constants reported by Gannett & Sura[16] (higher association constant for the 8-OG:G mismatch

Table 2. Melting temperatures determined by UV absorbance for dodecamer duplexes

Duplex	t_m (°C)
G:C	55.4[a]
G:G mismatch	23.6[a]
A:8-OG mismatch	47.5
G:8-OG mismatch	52.8

Dodecamer duplex with the d(CGCXAATTYGCG)$_2$ sequence, where X and Y are the residues listed in the Table.

[a] Values reported by Borden *et al.*,[30] obtained under similar conditions.

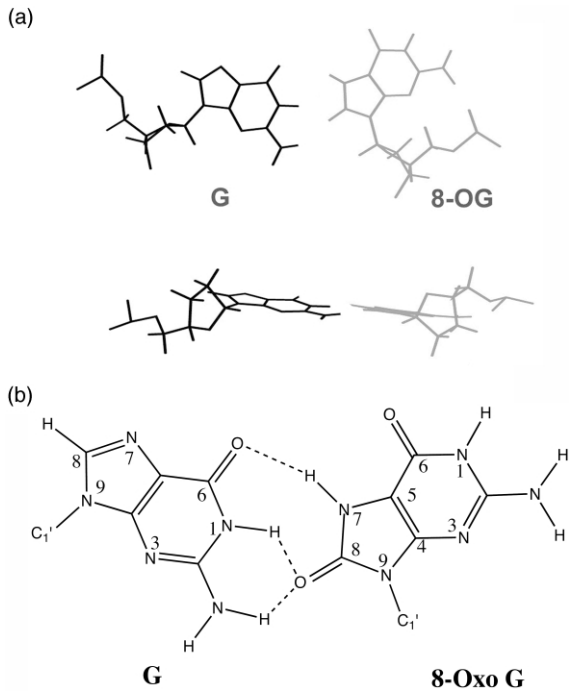

Figure 5. (a) Refined structure of the 8-OG:G mismatched duplex, viewed along the helical axis, showing the 8-OG:G base mis-pair. (b) A diagram of the 8-OG:G mis-pair showing the three-centered hydrogen bonding between the O8 of the 8-OG residue at the amino and imino protons of the G residue.

than for the 8-OG:A mismatch), indicate that the 8-OG:G mismatch is more stable than the 8-OG:A mismatch. The association constants reported for the 8-OG:G mismatch is higher than the values for the 8-OG:A and 8-OG:T mismatches but lower than the value for the 8-OG:C base-pair. The t_m of the 8-OG:G-containing duplex is only 2.6 deg. C lower than the t_m observed for the unmodified (G:C) duplex. Since the perturbation caused by the modification is small, it is possible that this modification could go un-repaired, resulting in G:C to C:G transversions.

The *syn* conformation of 8-oxo-G

Bulky substitution at the C-8 position is thought to switch the glycosidic torsional angle in the guanine nucleotide to adopt a *syn* conformation.[33] However, the observation of the *syn* conformation in some of the G:G mismatches and the observation of *anti* glycosidic angles in the 8OG:C mismatches in both the X-ray crystal and NMR solution structures, suggest that the "bulky-substitution" at the C-8 position may not be the sole determinant of the *syn–anti* switch. The hydrogen bonding pattern between the paired residues plays a significant role in determining the *syn–anti* conformation. The oxidation of a G residue alters the arrangement of hydrogen bond donor/acceptor positions, and allows the 8-OG to form hydrogen bonds that are different from the normal Watson–Crick bonding pattern observed in G:C base-pairs. This would explain the *anti* glycosidic bond for the 8OG when it is paired with C, where normal Watson–Crick base-pairing can occur between the two bases with three hydrogen bonds. With A and G, the 8-OG is forced to switch to the *syn* conformation to best accommodate the hydrogen bonding. The *syn* confirmation of the 8-OG orients the Hoogsteen edge of the residue towards the center of the duplex, enabling the formation of hydrogen bonds, and thereby offsets the higher energy of the *syn* conformation. In the *anti* conformation, the 8-OG would pair with C without changing the Watson-Crick hydrogen bonding pattern observed in the G:C base-pair. Therefore, the conformational preference of the 8-OG residue in a duplex DNA appears to be determined by the interplay of the total number of hydrogen bonds and the steric interaction between the O at C-8 postion and the H2″ proton.

Bifurcated hydrogen stabilizes the 8-OG:G base-pair

The 8-OG:G base-pair is stabilized by two hydrogen bonding interactions (Figure 5). The first hydrogen bond forms between the carbonyl oxygen atom of G and the H7 of the 8-OG residue. The C═O···H distance for this interaction is 1.9(± 0.3) Å. The second hydrogen bonding interaction, which we propose on the basis of the final averaged structure, is a three-centered hydrogen bond where the O8 of the 8-OG residue interacts with the H1 as well as with an amino proton of the G (Figure 5). In several crystal structures of organic molecules, the carbonyl oxygen atoms are reported to be involved in hydrogen bonding interactions with two different hydrogen atoms.[34] In the crystal structure reported for a DNA duplex containing an 8-oxo adenine:G mismatch,[35] the 8-OA:G base-pair is held together by two, three-centered hydrogen bonds. The three-centered hydrogen bonds are thought to remove the destabilizing effect caused by the presence of a completely unfulfilled hydrogen bond donor, i.e. the N2 amino group in the 8-OG residue. The three-centered hydrogen bonds involving carbonyl oxygen atoms are considered to be real if the H···O distances are short enough and the C═O···H angle is greater than 90°.[36] In the final averaged structure, the distances are 1.84 Å (to the H1 imino) and 2.24 Å (to the amino H). As in the 8-OA:G structure,[35] the three-centered hydrogen bond between O8 of 8-OG and the imino and amino protons of G, alleviate the destabilization of the base-pair that is likely to be caused by the presence of an unfulfilled hydrogen bond donor, i.e. the N2 amino group. The higher t_m observed for the 8-OG:G mismatch compared to the 8-OG:A mismatch indicates the higher thermal stability of the 8-OG:G mismatch. The extra stability may arise from the bifurcated hydrogen bond observed in the 8-OG:G mismatch.

Materials and Methods

Synthesis of 8-OG containing duplex

The 12-mer oligonucleotides, d(CGCGAATT$^{8\text{-O}}$GGCG) at 15 μM scale and d(CGCAAATT$^{8\text{-O}}$GGCG) at 0.2 μM scale, were synthesized by the phosphoramidite method on an ABI Expedite model 8900 DNA synthesizer using 8-oxo-dG-CE phosphoramidite (Glen Research) with off-line coupling of the reagent. The 5′-dimethoxytrityl (DMT)-oligonucleotides were cleaved from the solid support and the base-protecting groups were removed using concentrated NH_4OH containing 0.25 M 2-mercaptoethanol (16 hours at 55 °C). The full-length 5′-DMT-protected oligonucleotides were separated from failure sequences using a C-18 Sep-Pak column (Waters Corp.) followed by removal of the 5′DMTgroup with 1% (v/v) aqueous trifluoroacetic acid (TFA) and elution of the product with 20% (v/v) acetonitrile. The oligonucleotides were purified further by reverse-phase HPLC using a Waters Delta-Pak C-18 column and gradient elution (0–20% acetonitrile, 20 minutes in 0.1 M triethylamine acetate (TEAA) buffer, pH 7.2). The products were then dialyzed against 10 mM NaCl and once again in distilled water before final lyophilization.

Sample preparation

Purity of the oligonucleotides was assessed by HPLC and NMR. The sample was lyophilized and dissolved in phosphate buffer (10 mM sodium phosphate (pH 6.8), 0.05 mM EDTA, 100 mM NaCl). For the NMR experiments in ^2H_2O solvent, the sample was lyophilized and re-dissolved in 99.996% ^2H_2O. The sample was heated to 90 °C for two minutes and cooled slowly to room temperature, to ensure the formation of the duplex. The final concentration of DNA in the sample, calculated from UV absorbance measurements, was about 2 mM.

NMR experiments

All proton NMR experiments were done at 750 MHz on a Varian UnityPlus instrument equipped with pulsed field gradients. Phase-sensitive two-dimensional NOESY spectra in ^2H_2O were collected at 10 °C, and 25 °C using a spectral width of 5000 Hz and mixing times of 50 ms and 250 ms. The real and imaginary data points were acquired sequentially. The data sets were collected with 512 t_1 experiments using 2048 complex points in the t_2 dimension and 32 scans per t_1 increment. The relaxation delay was three seconds. Two-dimensional NOESY data in H_2O were collected at 10 °C with the spectral width of 15,000 Hz and a mixing time of 250 ms. The H_2O peak was suppressed by a combination of soft 90° shaped pulses and *z*-gradient pulses during the mixing time. Other acquisition parameters were the same as for the ^2H_2O spectra.

Two-dimensional double quantum filtered correlated spectroscopy (DQF-COSY) and TOCSY data at 25 °C were collected with a spectral width of 4400 Hz and 30 ms and 80 ms spin-lock mixing times (TOCSY experiment). The data sets were collected with 2048 complex points in the t_2 dimension and 256 t_1 increments. Phosphorus spectra in ^2H_2O at 25 °C were obtained at 240 MHz on a Varian UnityPlus 600 instrument using a broad-band probe (Nalorac). A 2D $^1H/^{31}P$ heteronuclear correlation experiment,[25] and a series of 1D ^{31}P spectra at different temperatures were collected at 240 MHz on a Varian UnityPlus-600 instrument. The ^{31}P resonances are referenced to trimethylphosphate (TMP), at 0.00 ppm, which resonates 3.456 ppm downfield of 85% (v/v) phosphoric acid.

The data sets were processed using VNMR (Varian). The 2D data sets were zero-filled in both dimensions, and were apodized with a 90°-shifted sine bell window function before Fourier transformation.

Distance restraints

Using the iterative hybrid relaxation matrix program, MORASS†,[37] and the intra-residue cytosine H5-H6 volumes as the ruler, distance restraints were calculated from the volumes of the 2D-NOESY cross-peaks between non-exchangeable protons. NOE spectra were simulated from starting model structures at 200 ms mixing time assuming an isotropic correlation time of 2.8 ns. A hybrid of experimentally determined NOESY cross-peak volumes and calculated NOESY volume matrix of starting geometry was built to approximate a complete experimental NOESY volume matrix. The cross-relaxation rate for each proton pair was then calculated with multiple spin effects treated explicitly. Inter-proton distances were calculated from the cross-relaxation rates, assuming a simple isotropic spectral density function. Distances involving exchangeable protons were estimated qualitatively from the NOESY peaks as weak (1.9–5.5 Å), medium (1.9–4.5 Å), or strong (1.9–3.5 Å). Watson–Crick base-pairing hydrogen bond restraints were added between the base-pairs in the duplex, at an equilibrium distance of 1.9(± 0.19) Å with a force constant of 15 kcal/mol Å^2. Only one hydrogen bond restraint was applied to both AT (between N1 of A and H3 of T) and GC base-pairs (between H1 of G and N3 of C) to allow variable propeller twist between the base-pairs during the refinement. No hydrogen bonding restraint was added for the G:8-OG base-pairs.

Structure refinement

An initial model structure, with the 8-OG residue in a *syn* conformation, was constructed using the xLEAP in the molecular mechanics/dynamics program AMBER5.0‡, and was subjected to energy minimization to remove any unfavorable van der Waals contacts. Partial atomic charges on 8-OG were generated for the AMBER forcefield by calculating the electrostatic potentials using Gaussian 94 with a 6-31G* basis set then using these data as input to the RESP utility in AMBER5.0. These parameter libraries are available from the authors. The starting structure was placed in a rectangular box, providing at least 12 Å of explicit triangulated three-point water molecules around each DNA molecule, yielding 4692 water molecules. To neutralize the charges on phosphate groups, 22 sodium ions were placed around the negatively charged phosphate groups in the phosphodiester backbone. Constant pressure was maintained with isotropic scaling. First, the water box was subjected to a series of equilibration molecular dynamics (MD) runs while holding the solute fixed.[38] Position constraints on solute molecules were relaxed gradually during the equilibration steps performed using the particle mesh Ewald (PME) method to

† http://www.nmr.utmb.edu/#mrass
‡ http://www.amber.ucsf.edu/amber

calculate electrostatic interactions.[39] The resulting structure was used as the starting structure for the subsequent rounds of refinement using restrained MD (r-MD).

The errors (i.e. uncertainties) in the calculated proton–proton distances were described using a flat-well energy penalty function in which the width of the flat-well is defined as a percentage of the equilibrium inter proton distance, r_{ij}^{eq}. The effect of force constant on the distance restraints was controlled by changing the error bars from an initial value of $\pm 25\%$ r_{ij}^{eq} to ca 10%, while the distance restraint force constants were increased accordingly as the confidence in the intermediate structures was established.

During r-MD, the non-bonded interaction cutoff distance was set to 10 Å and a distance-dependent dielectric constant was used with an integration time step of 1 fs. Coordinates were stored every 50 steps. The charges at the 5′ and 3′ ends of the DNA strands were modified to avoid non-physical electrostatic interactions.

For each iteration, the starting structure was subjected to 8 ps of r-MD with temperature annealing (increasing the temperature from 298 K to 600 K for 2 ps, cooling to 298 K over the next 3 ps, continuing at 298 K for the last 3 ps). The average structure from the last 3 ps of r-MD was energy-minimized for 2000 steps without restraints, and the resulting structure was used as the starting structure for the next iteration of MORASS/r-MD.

The progress of the iterative refinement process to convergence was monitored by several key indicators, as defined below, which are listed in Table 1:

$$\%\mathrm{rms(volume)} = \sqrt{1/N \sum_{ij} \left(\frac{v_{ij}^a - v_{ij}^b}{v_{ij}^a} \right)^2} \times 100\%$$

$$R = \frac{\sum_{ij} \left| v_{ij}^a - v_{ij}^b \right|}{\sum_{ij} v_{ij}^a}$$

$$Q(1/6) = \frac{\sum_{ij} \tau_m \left| (v_{ij}^a)^{1/6} - (v_{ij}^b)^{1/6} \right|}{\sum_{ij} (1/2) \tau_m \left| (v_{ij}^a)^{1/6} + (v_{ij}^b)^{1/6} \right|}$$

where v_{ij} is the 2D NOESY volume and a and b can be theoretical or experimental volumes. The τ_m is the NOESY mixing time.

The final structure obtained from the last iterative 8 ps r-MD refinement was subjected to a 20 ps r-MD. The 20 lowest-energy structures, during the last 3 ps of this r-MD, were selected and averaged to the single structure shown in Figure 4.

The helical parameters and the dihedral angles of the final averaged structure were calculated using the CURVES program.[28] All structures were displayed with MIDAS2.1.[40]

UV-melting experiments

Melting curves were recorded at 260 nm using a Cary 1-Bio spectrophotometer (Varian Associates) equipped with a temperature-controller using circulating water heater/cooler unit. Oligonucleotide samples were prepared in 10 mM sodium phosphate (pH 6.8), 100 mM KCl, 0.05 mM EDTA. The concentration of the duplex was 1 μM. Samples were heated to 95 °C for three minutes and cooled slowly to room temperature to ensure annealing of the strands. The absorbance at 260 nm was monitored every 0.5 deg. C, from 25 °C to 95 °C. The heating rate was set at 1 deg. C/minute. Samples were allowed to equilibrate at the starting temperature until the absorbance remained constant for at least ten minutes. Cuvettes were sealed to prevent sample evaporation. Melting temperatures were calculated from the sigmoid melting curves using a two-state model that assumes a simple equilibrium between the duplex and the single-stranded forms.

Protein Data Bank accession numbers

Coordinates are available from the Protein Data Bank (PDB): 1N2W.

Acknowledgements

This research was supported by NIH (ES06839 and 1P30 ES06676), and Welch Foundation (H-1296) grants (to D.G.G.), US Public Health Service grants CA81063 and NIEHS Center grant ES06676 (to S.M.). The authors thank Dr Richard Hodge for the synthesis of oligonucleotides used in this study.

References

1. Culp, S. J., Cho, B. P., Kadlubar, F. F. & Evans, F. E. (1989). Structural and conformational analyses of 8-hydroxy-2′-deoxyguanosine. *Chem. Res. Toxicol.* **2**, 416–422.
2. Cho, B. P. & Evans, F. E. (1991). Structure of oxidatively damaged nucleic acid adducts: tautomerism, ionization and protonation of 8-hydroxyadenosine studied by ^{15}N NMR spectroscopy. *Nucl. Acids Res.* **19**, 1041–1047.
3. Malins, D. C., Polissar, N. L., Ostrander, G. K. & Vinson, M. A. (2000). Single 8-oxo-guanine and 8-oxo-adenine lesions induce marked changes in the backbone structure of a 25-base DNA strand. *Proc. Natl Acad. Sci. USA*, **97**, 12442–12445.
4. Kuchino, Y., Mori, F., Kasai, H., Inoue, H., Iwai, S., Miura, K. *et al.* (1987). Misreading of DNA templates containing 8-hydroxydeoxyguanosine at the modified base and at adjacent residues. *Nature*, **327**, 77–79.
5. Shibutani, S., Takeshita, M. & Grollman, A. P. (1991). Insertion of specific bases during DNA synthesis past the oxidation-damaged base 8-oxodG. *Nature*, **349**, 431–434.
6. Sargentini, N. J. & Smith, K. C. (1994). DNA sequence analysis of spontaneous and gamma-radiation (anoxic)-induced lacId mutations in *Escherichia coli* umuC122 :: Tn5: differential requirement for umuC at G·C *versus* A·T sites and for the production of transversions *versus* transitions. *Mutat Res.* **311**, 175–189.
7. Buchko, G. W., Wagner, J. R., Cadet, J., Raoul, S. & Weinfeld, M. (1995). Methylene blue-mediated photo-oxidation of 7,8-dihydro-8-oxo-2′-deoxyguanosine. *Biochem. Biophys. Acta*, **1263**, 17–24.
8. Hazra, T. K., Izumi, T., Maidt, L., Floyd, R. A. & Mitra, S. (1998). The presence of two distinct 8-oxoguanine repair enzyme in human cells: their complimentary roles in preventing mutation. *Nucl. Acids Res.* **26**, 5116–5122.

9. Zhang, Q. M., Ishikawa, N., Nakahara, T. & Yonei, S. (1998). *Escherichia coli* MutY protein has a guanine-DNA glycosylase that acts on 7,8-dihydro-8-oxoguanine:guanine mispair to prevent spontaneous G:C → C:G transversions. *Nucl. Acids Res.* **26**, 4669–4675.
10. Duarte, V., Muller, J. G. & Burrows, C. J. (1999). Insertion of dGMP and damp during *in vitro* DNA synthesis opposite an oxidized form of 7,8-dihydro-8-oxoguanine. *Nucl. Acids Res.* **27**, 2247–2249.
11. Hazra, T. K., Muller, J. G., Manuel, R. C., Burrows, C. J., Lloyd, R. S. & Mitra, S. (2001). Repair of hydantoins, one electron oxidation product of 8-oxoguanine, by DNA glycosylases of *Escherichia coli*. *Nucl. Acids Res.* **29**, 1967–1974.
12. Kouchakdjian, M., Bodepudi, V., Shibutani, S., Eisenberg, M., Johnson, F., Grollman, A. P. & Patel, D. J. (1991). NMR structural studies of the ionizing radiation adduct 7-hydro-8-oxodeoxyguanosine (8-oxo-7H-dG). opposite deoxyadenosine in a DNA duplex. 8-oxo-7H-dG(syn):dA(anti). alignment at lesion site. *Biochemistry*, **30**, 1403–1412.
13. McAuley-Hecht, K. E., Leonard, G. A., Gibson, N. J., Thomson, J. B., Watson, W. P., Hunter, W. N. & Brown, T. (1994). Crystal structure of a DNA duplex containing 8-hydroxydeoxyguanine-adenine base-pairs. *Biochemistry*, **33**, 10266–10270.
14. Lipscomb, L. A., Peek, M. E., Morningstar, M. L., Verghis, S. M., Miller, E. M., Rich, A. *et al.* (1995). X-ray structure of a DNA decamer containing 7,8-dihydro-8-oxoguanine. *Proc. Natl Acad. Sci. USA*, **92**, 719–723.
15. Oda, Y., Uesugi, S., Ikehara, M., Nishimura, S., Kawase, Y., Ishikawa, H. *et al.* (1991). NMR studies of a DNA containing 8-hydroxydeoxyguanosine. *Nucl. Acids Res.* **19**, 1407–1412.
16. Gannett, P. M. & Sura, T. P. (1993). Base-pairing of 8-oxoguanosine and 8-oxo-2′-deoxyguanosine with 2′-deoxyadenosine, 2′-deoxycytosine, 2′-deoxyguanosine, and thymidine. *Chem. Res. Toxicol.* **6**, 690–700.
17. Dickerson, R. E. & Drew, H. R. (1981). Structure of a B-DNA dodecamer. II. Influence of base sequence on helix structure. *J. Mol. Biol.* **149**, 761–786.
18. Chiu, T. K., Kaczor-Grzeskowiak, M. & Dickerson, R. E. (1999). Absence of minor groove monovalent cations in the crosslinked dodecamer C-G-C-G-A-A-T-T-C-G-C-G. *J. Mol. Biol.* **292**, 589–608.
19. Wellenzohn, B., Flader, W., Winger, R. H., Hallbrucker, A., Mayer, E. & Liedl, K. R. (2001). Exocyclic groups in the minor groove influence the backbone conformation of DNA. *Nucl. Acids Res.* **29**, 5036–5043.
20. Wüthrich, K. (1986). *NMR of Proteins and Nucleic Acids*, Wiley, New York, NY.
21. Ikehara, M., Uesugi, S. & Yoshida, K. (1972). Studies on the conformation of purine nucleosides and their 5′-phosphates. *Biochemistry*, **11**, 830–836.
22. Uesugi, S. & Ikehara, M. (1977). Carbon-13 magnetic resonance spectra of 8-substituted purine nucleosides. Characteristic shifts for the *syn* conformation. *J. Am. Chem. Soc.* **99**, 3250–3253.
23. Gorenstein, D. G., Schroeder, S. A., Fu, J. M., Metz, J. T., Roongta, V. & Jones, C. R. (1988). Assignment of ^{31}P NMR resonances in oligodeoxyribonucleotides: origin of sequence specific variations in the deoxyribose phosphate backbone conformation and the ^{31}P chemical shifts of double-helical nucleic acids. *Biochemistry*, **27**, 7223–7237.
24. Roongta, V. A., Jones, C. R. & Gorenstein, D. G. (1990). Effect of Distortions in the deoxyribose phosphate backbone conformation of duplex oligodeoxyribonucleotide dodecamers containing GT, GG, GA, AC, and GU base-pair mismatches on ^{31}P NMR spectra. *Biochemistry*, **29**, 5245–5258.
25. Kellogg, G. W. (1992). Proton-detected hetero-TOCSY experiments with application to nucleic acids. *J. Magn. Reson.* **98**, 176–182.
26. Nikonowicz, E., Roongta, V. A., Jones, C. R. & Gorenstein, D. G. (1989). Two-dimensional H-1 and P-31 NMR spectra and restrained molecular dynamics structure of an extrahelical adenosine tridecamer oligodeoxyribonucleotide duplex. *Biochemistry*, **28**, 8714–8725.
27. Gorenstein, D. G., Meadows, R. P., Metz, J. T., Nikonowicz, E. & Post, C. B. (1990). ^{31}P and ^{1}H 2-dimensional NMR and NOESY-distance restrained molecular dynamics methodology for defining sequence-specific variations in duplex oligonucleotides; a comparison of NOESY two-spin and relaxation rate matrix analysis. In *Advances in Biophysical Chemistry* (Bush, C. A., ed.), pp. 47–124, JAI Press, Greenwich, CT.
28. Lavery, R. & Sklenar, H. (1988). The definition of generalized helicoidal parameters and of axis curvature for irregular nucleic acids. *J. Biomol. Struct. Dynam.* **6**, 63–91.
29. Gorenstein, D. G. (1994). Conformation and dynamics of DNA and protein–DNA complexes by ^{31}P NMR. *Chem. Rev.* **94**, 1315–1338.
30. Borden, K. L. B., Jenkins, T. C., Skelly, J. V., Brown, T. & Lane, A. N. (1992). Conformational properties of the G-G mismatch in d(CGCGAATTGGCG) 2 determined by NMR. *Biochemistry*, **31**, 5411–5421.
31. Topal, M. D. & Fresco, J. R. (1976). Complementary base-pairing and the origin of substitution mutations. *Nature*, **263**, 285–289.
32. Cognet, J. A., Gabarro-Arpa, J., Le Bret, M., van der Marel, G. A., van Boom, J. H. & Fazakerley, G. V. (1991). Solution conformation of an oligonucleotide containing a G·G mismatch determined by nuclear magnetic resonance and molecular mechanics. *Nucl. Acids Res.* **25**, 6771–6779.
33. Saenger, W. (1984). *Principles of Nucleic Acid Structure*, Springer, New York.
34. Taylor, R., Kennard, O. & Versichel, W. (1983). Geometry of the N–H···O═C bond. Lone-pair directionality. *J. Am. Chem. Soc.* **105**, 5761–5766.
35. Leonard, G. A., Guy, A., Brown, T., Teoule, R. & Hunter, W. N. (1992). Conformation of guanine-8-oxoadenine base-pairs in the crystal structure of d(CGCGAATT(O8A)GCG). *Biochemistry*, **31**, 8415–8420.
36. Taylor, R., Kennard, O. & Versichel, W. (1984). Geometry of the N–H···O═C bond. Three-center and four-center bonds. *J. Am. Chem. Soc.* **106**, 244–248.
37. Post, C. B., Meadows, R. P. & Gorenstein, D. G. (1990). On the evaluation of interproton distances for three-dimensional structural analysis by NMR using a relaxation rate matrix analysis. *J. Am. Chem. Soc.* **112**, 6796–6803.
38. Cheatham, T. E., Miller, J. L., Fox, T., Darden, T. A. & Kollman, P. A. (1995). Molecular dynamics simulations on solvated biomolecular systems. *J. Am. Chem. Soc.* **117**, 4193–4194.
39. Darden, T. A., York, D. & Pedersen, L. G. (1993). Particle Mesh Ewald—an $n\log(n)$ method for

Ewald sums in large systems. *J. Chem. Phys.* **98**, 10089–10092.
40. Ferrin, T. E., Huang, C. C., Jarvis, L. E. & Langridge, R. (1988). The MIDAS display system. *J. Mol. Graphics*, **6**, 13–37.

Edited by P. J. Hagerman

(Received 12 August 2002; received in revised form 31 October 2002; accepted 31 October 2002)

SCIENCE DIRECT®
www.sciencedirect.com

Supplementary Material comprising two Tables is available